HHS Public Access

Author manuscript

ACS Appl Bio Mater. Author manuscript; available in PMC 2023 April 06.

Published in final edited form as:

ACS Appl Bio Mater. 2019 November 18; 2(11): 4826–4836. doi:10.1021/acsabm.9b00592.

MRI-Guided, Noninvasive Delivery of Magneto-Electric Drug Nanocarriers to the Brain in a Nonhuman Primate

Ajeet Kaushik[*,†,△], **Jose Rodriguez**[‡], **Dan Rothen**[§], **Vinay Bhardwaj**[‖], **Rahul Dev Jayant**[⊥], **Pradip Pattany**[§], **Beatriz Fuentes**[§], **Hitendra Chand**[†], **Nagesh Kolishetti**[†], **Nazira El-Hage**[†], **Kamel Khalili**[#], **Norma S. Kenyon**[¶], **Madhavan Nair**[*,†]

[†]Center of Personalized Nanomedicine, Institute of Neuroimmune Pharmacology, Department of Immunology and Nano-Medicine, Herbert Wertheim College of Medicine, Florida International University, Miami, Florida 33199, United States

[‡]Interdisciplinary Stem Cell Institute

[§]Division of Veterinary Resources, Miller School of Medicine, University of Miami, Miami, Florida 33136, United States

[‖]Department of Biomedical Engineering, Rutgers University, Piscataway, New Jersey 08901, United States

[⊥]Department of Pharmaceutical Sciences, School of Pharmacy, Texas Tech University Health Sciences Center, Amarillo, Texas 79106, United States

[#]Department of Neuroscience, Lewis Katz School of Medicine, Temple University, Philadelphia, Pennsylvania 19140, United States

[¶]Cell Transplant Center, Diabetes Research Institute, Miller School of Medicine University of Miami, Miami, Florida 33136, United States

Abstract

[*]**Corresponding Authors** ajeet.npl@gmail.com (AK). nairm@fiu.edu (MN).

[△]**Present Address** Department of Natural Sciences, Division of Sciences, Arts and Mathematics (SAM), Florida Polytechnic University, Lakeland, FL 33805-8531, USA.

Author Contributions

A.K. designed and coordinated research and was actively involved in all experiments, data analysis, and manuscript writing; J.R. performed all MRI-related experiments; D.R. performed baboon-related experiments; V.B. performed Raman microscopy and spectroscopy; R.J.D. assisted in MENP characterization, protocol optimization, and magnetically guided brain delivery; P.P. assisted in MRI studies and image analysis; B.F. assisted D.R. for MENP injection in the baboon and related experiments; H.C. contributed to analyzing Raman microscopy; N.K. assisted in exploring biosafety aspects of MENPs; N.E.-H. assisted in H&E imaging and explained organ morphology; K.K. and N.S.K. contributed to planning baboon-related experiments; M.N. was involved in all research, discussion, planning, and continuous supervision.

The authors declare no competing financial interest.

ASSOCIATED CONTENT

Supporting Information

The Supporting Information is available free of charge on the ACS Publications website at DOI: 10.1021/acsabm.9b00592.

Supplementary Figure 1: Characterization of MENPs and magnetically guided delivery to the mice brain. XRD pattern of MENPs showing peaks corresponding to CFO and BTO confirming crystalline core–shell composition of MENPs (a). TEM image of MENPs showing average particle size of ~25 nm (b). The MTT assay study for the cell viability assessment as a function of varying MENP concentration using primary human astrocytes (c) and SMNMC (d) cells. Representation of the brain delivery MENPs (5 mg/kg) under influence of 3 h static magnetic field exposure (e) (PDF)

A magnetically guided brain delivery method previously demonstrated in mice has not yet been translated for clinical applications due to the mismatch of available static magnet dimensions in relation to the human brain size and shape. To develop a human-compatible methodology, we explored magnetic resonance imaging (MRI) as a tool for the delivery of magneto-electric nanoparticles (MENPs) into the brain of a baboon, as a proof-of-concept study. MRI brain image analysis showed a reduction in T_2* value at the basal ganglia, hemisphere, and vertex, thereby confirming successful MENP delivery to the brain. The observation of well-integrated morphologically healthy tissues and no blood toxicity over the study duration confirmed the biocompatibility of MENPs and the delivery procedure. Outcomes of this research present MRI-assisted delivery of MENPs to the brain as a safe and noninvasive method in larger species such as baboons and one step closer to human translation. This MENP-based nanomedicine delivery method can be used for clinical application in order to investigate effective central nervous system (CNS) therapies.

Graphical Abstract

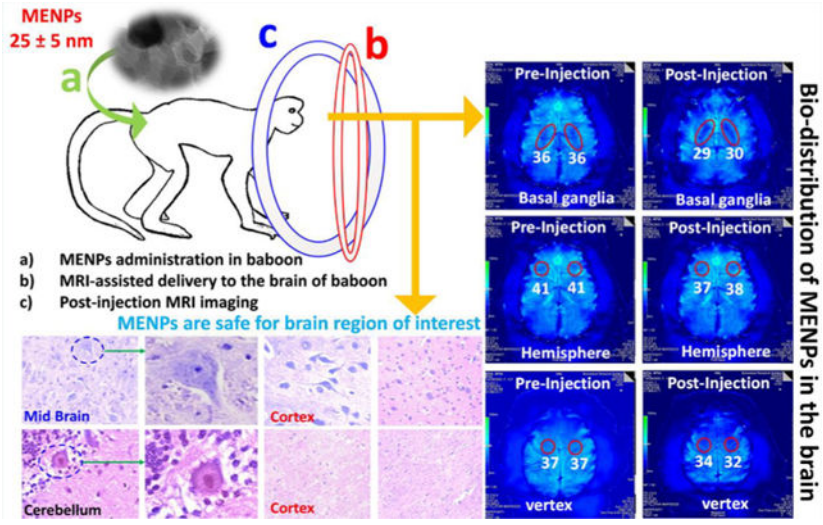

Keywords

brain delivery; drug nanocarriers; magneto-electro nanoparticles (MENPs); personalized nanomedicine; magnetic resonance imaging (MRI)

INTRODUCTION

A safe and effective brain delivery method for delivery of specific therapeutic agents to cure diseases of the central nervous system (CNS) is an unmet need.[1–3] The incidences of these diseases are growing rapidly, resulting in billions of dollars of socio-economic burden.[4–6] The treatment and management of CNS diseases which consist of predominately brain tumors and neurocognitive disorders, including Parkinson's disease, Alzheimer's disease, and neuro-HIV/AIDS, requires promising therapeutics development.[6–8] Despite significant advances in the development of novel, targeted drugs with improved therapeutic activity, the complete treatment or eradication of CNS diseases has not been fully achieved.[6] This

is largely due to the inability of many of the currently effective therapeutic drugs to cross the blood–brain barrier (BBB).[9,10] The approach of developing pharmacologically relevant, therapeutic cargos and assemblies (i.e., nanomedicine with the ability to cross the BBB) has been performed and has shown good promise toward the treatment of some CNS diseases. To develop a personalized nanomedicine, various methodologies are utilized to achieve the following goals: (a) to prepare a specific therapeutic formulation for a target disease, (b) the delivery of a pharmacologically relevant formulation across the BBB safely and without side effects, and (c) the scaling up of all available approaches to advance *in vivo* to clinical-phase research.[4,9,11] Additionally, the development of a noninvasive brain delivery method, without adverse clinical effects, is critical and in high demand.[1] Considering the current environment for research and its associated challenges, current therapeutic formulations have shown limited delivery across the BBB (with the additional rare presence of off-targeting), or these previous methods have shown adverse side effects including toxicity and altered neurobehavioral (motor coordination) functions.[1,3] For example, site-specific therapeutic agents prepared using proteins or antibodies are considerably larger in size and have shown low efficacy for brain delivery.[1,3] The use of external stimulation, such as focused ultrasound or electric field, transiently opens the BBB, thereby allowing nonselective delivery of potentially undesirable compounds to the brain that could ultimately lead to neurologic inflammation and subsequent inflammatory-induced neurologic disorders. These stimulation methods are known to affect motor coordination and thus motor function in animals.[2,3,12] Therefore, the investigation of novel nanoformulations (NFs) having specific therapeutic functions is crucial for the development of safe and efficacious brain therapies and the continued advancement of personalized medicine.

Among the various, reported methodologies, static magnetic-field-based, magnetically guided brain delivery methods have been reported to be safe and noninvasive.[6,7,12] Successful delivery of drug-laden nanocarriers (NCs) to the brain of mice has already been demonstrated using this technique.[12] This method seems suitable and appropriate for the delivery of magnetic, drug-loaded NFs into the CNS to provide maximum efficacy in combating specific neurologic diseases. Using this described methodology, the expectation is that the delivered therapeutics will have very little to no adverse effects on the patient in terms of toxicity, motor coordination, and motor function. In prior studies by our research group and utilizing the same methodology, we demonstrated efficacious brain delivery of magneto-electro nanoparticles (MENPs) in mice. The surface charges for the ferromagnetic nanoparticles (MENPs) were cationic (25 ± 5 nm) and exhibited the following prominent features: (a) binding with specific drugs (anti-HIV,[13] anticancer,[12] siRNA,[14] Cas9/gRNA[3]), (b) the ability to cross the BBB under the influence of a static magnetic field, and (c) the on-demand release of a drug after exposure to alternating current (A/C) magnetic field stimulation using an electromagnetic coil.[3,9,15] Recently, MENPs have been shown to be suitable NCs for drugs for CNS delivery in mice, with a static magnetic field of 0.8 T.[1] The microscopic analysis of MENPs injected into the brains of mice showed uniform distribution of MENPs throughout all brain cell types, without compromising their chemical integrity.[16] There was no observation of tissue- nor blood-specific toxicity, suggesting wide safety margins of the applied magnetic field and the MENPs. A behavioral assessment of these mice confirmed that there was no noticeable change in motor coordination or

function over time after the MENP administration.[1] Magnetically guided brain delivery was successful in small animals but had additional challenges when attempting to translate this methodology into a clinical utility. This is due to a dimensional mismatch among static magnets and size dimensions in relation to human brain size and shape. Unfortunately, a human-compatible, magnetically guided, safe, and noninvasive brain delivery method has not yet been developed. However, such methods are of critical need to develop personalized nanomedicine and the management of CNS diseases.

Magnetic resonance imaging (MRI) is in practice as a safe analytical tool for disease diagnostics, clinical monitoring, therapeutic decision-making, efficacy of therapy, and health care management.[17] Specifically, in relation to CNS disease and pathology, MRI is one of the most successful clinical technologies utilized by neurologists and neurosurgeons to diagnose, locate, and potentially treat brain tumors. Raman spectroscopy can be integrated with MRI in the clinical diagnostic procedure to allow surgeons to make real-time decisions during the surgery (intraoperative) as MRI is strictly a pre-/postoperative diagnostic tool.[18,19]

Besides significant achievements in CNS imaging, the magnetic field of the MRI instrument has been used for various therapeutic purposes;[20,21] for example, the static magnetic field of an MRI demonstrated beneficial brain stimulation,[22] stimulation of rotational sensors in the brain,[12] and vestibular stimulation.[23] Considering the aforementioned features, this pilot project explored the MRI as a tool to achieve effective delivery of magnetically guided MENPs to the brain of an adult Hamadryas baboon (*Papio hamadryas*). The results of MRI brain imaging confirmed distribution of MENPs in the basal ganglia, hemisphere, and vertex regions of the brain. The histopathologic analyses (brain and other major organs), clinical chemistry profile analyses (30 days follow up), and tissue integrity analyses by Raman spectroscopy showed no evidence of any adverse effects caused by MENP accumulation in the brain or to the other organs of the baboon. This showed promise for the potential for appropriate biosafety (biocompatibility and safety) of the MENPs in future clinical applications and that this successful, noninvasive brain delivery method should be further examined for clinical practicality to develop novel therapies to cure many different CNS diseases.

RESULTS AND DISCUSSION

The MENPs ($BaTiO_3$@$CoFe_2O_4$), composed of $BaTiO_3$ (BTO) as shell and $CoFe_2O_3$ (CFO) as core, are crystalline and of high purity, as confirmed by X-ray diffraction (XRD, Figure S1a in the Supporting Information). The average size of MENPs was 25 ± 5 nm as estimated by transmission electron microscopy (TEM, Figure S1b in the Supporting Information). The 3-(4,5-dimethylthiazol-2-yl)-2,5-diphenyl tetrazolium bromide (MTT, a colorimetric assay for assessing cell metabolic activity) cytotoxicity assay results showed a concentration of MENPs of up to 0.25 mg/mL (corresponding to a 10 mg/kg dose in mice) and cell viability of around 95% in primary human astrocytes (Figure S1c in the Supporting Information) and SKNMC (a neuroepithelioma cell line) cell lines (Figure S1d in the Supporting Information). Thus, an optimized 10 mg/kg concentration was diluted in 100 μL of PBS and administrated intravenously to mice for the magnetically guided brain

delivery (Figure S1e in the Supporting Information). The microscopic results of MENPs injected into the brains of mice showed uniform distribution of the MENPs in all regions of the brain and different cell types without any noticeable agglomeration.[1]

To overcome the inherent challenges of developing a mice-based brain delivery model for future clinical utility, a magnet of appropriate size in relation to human size is the bottlenecking requirement. We explored the static magnetic feature of an MRI instrument for this application. Prior to demonstrating MRI-assisted brain delivery of MENPs to nonhuman primates, an *ex vivo* phantom study was conducted to evaluate the variation in contrast in terms of T_2 value as a function of MENP concentration (Figure 1a). The results confirmed the magnitude of the T_2 (ms) value decreased with increasing MENP concentration (10 to 500 μg). A linear relationship (regression coefficient as 0.995) was observed between the $1/T_2$ value and MENP concentrations (Figure 1b). This correlation was useful to evaluate the MENP detection in a specific brain region of interest.

Magnetically guided delivery is a function of magnetic exposure time. To achieve the maximum efficacy of brain delivery while using the shortest possible magnetic exposure time is of the essence. Longer durations of magnetic exposure under anesthesia can lead to dizziness, delayed recovery, possibly altered motor coordination and function, and death.[24] The magnetically guided delivery of MENPs in the brains of mice as well as locations in the periphery (e.g., hepatic targeting) as a function of time (1 to 4 h) were assessed using *ex vivo* MRI (Figure 1c). The results of MRI of the brains showed that the T_2 value for the brain varies from 300 to 275 ms (1 h), 275 to 255 ms (2 h), 255 to 225 ms (3 h), and 225 to 220 ms (4 h) as a function of magnetic exposure time (Figure 1d). A significant difference in the T_2 value (around 2%) was not observed in the cases of 3 and 4 h magnetic exposure time. Therefore, we decided a 3 h static magnetic exposure was optimal to achieve the maximum brain delivery of nanoparticles. A similar trend was observed while analyzing the MRI results of MENP-injected mice livers. The T_2 value varied from 500 to 250 (ms) in the case of the liver (Figure 1b). The injected MENPs (3 h magnetic exposure time) were used to evaluate blood toxicity profiles, tissue morphology assessment, and evaluation of animal behavior.[1] Outcomes of these studies confirmed that there was no toxicity nor alteration in motor coordination and function due to the presence of MENPs.[1] Based on these results, 3 h of static magnetic field exposure was planned to achieve similar efficacy in the delivery of MENPs into the brain of a baboon using an MRI as a navigational tool without producing any undesirable side effects.

In this study, the MENP doses were calculated based on the surface area/body weight of the mouse or baboon. To develop the MENP-based nanoformulation for clinical translation, the nanoparticle dose optimization in mice and dose escalation in larger animal species (baboon) were calculated using *in silico* modeling.[25] Due to the differences between the absorption, distribution, metabolism, and excretion (ADME) behaviors of nanoparticles in mice vs the baboon, additional factors were also considered while building the physiologically based pharmacokinetic (PBPK) model for the MENP dose.

An MENP dose of 22 mg, with respect to 13 kg of body weight, was suspended in 100 mL of PBS and administrated intravenously (over 30 min) at a controlled rate using a peristaltic

syringe pump. The baboon was placed under a static magnetic field for MRI for 3 h (Figure 2a and 2b) to deliver MENPs across the BBB, and CNS delivery of MENPs was further confirmed by MRI imaging as compared with pre- and postinjection MRI images. The focus of this research is to explore MRI as a navigation tool to deliver across the BBB, and image analysis was utilized as a qualitative approach to understand biodistribution of MENPs in the brain. In addition, the evaluation of the biodistribution of MENPs in different regions of the brain and peripheral organs was also analyzed. The grayscale MRI image of the baboon organs recorded at pre- and postinjection did not show a significant T_2 value variation in the brain (Figure 2c) or periphery (Figure 2d). This is the reason that the T_2* mapping based MRI image processing was performed to provide the appropriate clarity needed to estimate variations which are dependent on the presence of MENPs. The mapping is an echo gradient based signaling and is more sensitive than T_2 (e.g., spin echo based signaling[26,27]). The variation in T_2* values can be correlated with the presence of iron. Higher iron concentration will lead to more reduction in the T_2* value.[26,27]

Our laboratory is actively involved in exploring nanoassisted technology to manage neuro-HIV. Keeping this view, the regions of interest (ROI) which are sensitive to HIV infection were selected for the analysis. Animal brain and other tissue scanning is routinely performed at the University of Miami facility, and the experts are capable of scanning the ROI properly. The results of the brain MRI images processed through T_2* mapping showed a reduction in T_2* value in basal ganglia from 36 to 29–30 (ms), the hemisphere (both) from 41 to 37–38 (ms), and the vertex from 36 to 29–30 (ms) (Figure 3a). This significant reduction in T_2* value confirms brain delivery of MENPs and effective distribution of the nanoparticles at important regions of interest which are highly significant for targeted CNS therapeutics. Though it is evident from MRI image analysis that MENPs were delivered to the brain of the baboon under the influence of an MRI magnetic field, there is a possibility that some MENPs are adhered to the walls. Besides this, 100% brain delivery seems impractical; therefore, investigating the distribution of MENPs in the periphery and any relatable side effects becomes imperative. Identical MRI image processing was used to analyze the baboon liver, kidneys, and spleen both pre and post MENPs injection (Figure 3b). The outcome of this analysis showed a significant T_2* reduction from 20 to 4.3 (ms) for the liver, 38 to 23 (ms) for the kidneys, and 18 to 4 (ms) for the spleen, thereby confirming the presence of MENPs in the animal's peripheral and highly vascular organs. MRI image analyses confirmed that magnetically guided brain delivery could be achieved using a static magnetic field of the MRI instrument with 3 h of exposure time. The presence of MENPs at the basal ganglia, hemisphere, and vertex regions of the brain makes these sensitive organs targetable for direct treatment using magnetic NFs based on iron particles bound with specific drugs or therapeutic compounds. Aiming to develop an MRI-assisted brain delivery system and to develop novel therapeutics for CNS diseases using MENP-based NFs, it was essential to look for any evidence of organ toxicity, tissue integration, and blood toxicity profiles due to the presence of MENPs.

It has been observed that inorganic nanoparticle administration in animals can cause time-dependent acute and chronic toxicity, leading to the secretion of inflammatory compounds that can subsequently result in neurocognitive disorders.[28–30] To investigate this, we explored the blood toxicity profile of intravenous MENPs in a baboon on days 2, 7, 14,

and 21. The parameters of renal and heaptic function along with other traditional analyses confirmed that all metabolic values were statistically within the same range as values obtained preinjection (Figure 4a). This confirmed a lack of any evidence of acute or chronic toxicity in the animal. Moreover, blood metabolic parameters obtained for the baboon pre and post MENP injection were also in agreement with physiological normal ranges (Figure 4b). However, segmented neutrophils and lymphocytes and glucose values were outside the physiological range, and this was related to the clinical history and duration of captivity of the baboon prior to MENP exposure.

Morphological analyses of tissues after ingestion or administration of nanocrystals (NCs) and specifically designed NFs due to nanoparticle diffusion or cell uptake are essential for safety assessment of these adopted methods and selected nanostructures or nanoassemblies.[31] The tissues can become damaged by interaction with nanoparticles and, if present, can lead to prolonged recovery. This could cause morphological defects and possibly the release of inflammatory mediators and cytokines due to the generation of acute-to-chronic toxicity. Hematoxylin and eosin (H&E) stain studies were conducted on samples of the major organs and tissues of the baboon including the brain and peripheral organs, 30 days post MENP injection (Figure 5, multiple images of the same organ, and only those selected are displayed). No morphological abnormalities were detected in tissues obtained from multiple areas of the brain including the midbrain, cerebellum, and cortex (Figure 5a). A representative, magnified image shows healthy neurons with prominent axons and dendrites in the midbrain and Purkinje neurons with a granular layer in the cerebellum, thereby confirming the biocompatibility of MENPs with respect to the nonhuman primate brain. The image analyses of major cortical regions showed well-aligned neuronal morphology, multipolar neurons, pyramidal neurons, spinal motor neurons, axons, satellite cells, connecting fibers, and capillary vessels, thus strongly suggesting there are no adverse effects from MENP administration and CNS delivery.

Considering that MENP elimination from the baboon is time dependent, the accumulation of MENPs should be at the highest levels in the periphery with less and less present in the brain. To further establish this, we selected the heart, lung, spleen, adrenal glands, uterus, kidneys, bladder, liver, stomach, and intestines for H&E staining (Figure 5b). A complete histopathologic analysis was performed by a veterinary pathologist, and this confirmed that there was no noticeable effect of MENP administration on tissue morphology. The results of the peripheral tissue analyses were confirmed with a blood toxicity profile, which also showed no significant observation of renal, hepatic, or other toxicity. Subclinical enteric inflammation was detected in the intestine of the baboon; however, this is likely due to the environmental effect of long-term indoor housing and is unrelated to the MENPs.

Raman spectral signatures were acquired to validate MENP biodistribution and biosafety assessment within baboon tissue samples. The excised tissues from various parts of the baboon’s brain and peripheral organs involved in the reticuloendothelial system (RES) clearance and excretory pathway were analyzed by Raman spectroscopy (Figure 6). The Raman fingerprint of the baboon brain is adapted from a technical bulletin released by Horiba Scientific explaining Raman imaging and spectroscopy of nonhuman primate brain tissue.[32] Besides this, the spectral features observed in MENP-injected baboon organs also

very closely resembled the MENPs[33] and nonhuman primates.[18] The presence of molecular signatures of highly conservative biomolecules and molecular bonds including collagen and amide III (1300 cm^{-1}), the CH_2 backbone of lipids and proteins (1450 cm^{-1}), and the C–C skeleton stretch in phospholipids and cholesterol (1000 to 1200 cm^{-1}) was the most dominant. The uptake and safety of the MENPs in the brain are confirmed by (a) dominance of all the characteristic peaks or signatures of life "organic molecules", (b) highly conserved molecular vibrations or signatures (Raman shift cm^{-1}) in reference to published Raman literature on animals and human brain tissue, and (c) complete discrimination of the Raman fingerprint of organic molecules from inorganic MENPs with the dominant metal signatures originating from $CoFe_2O_3$ and $BaTiO_3$ (600–800 cm^{-1}). The Raman spectral information on animal and human brains is used to differentiate between healthy and diseased neuronal cells (e.g., glioblastoma[18]) and injured neurons.[33] There was consistency in the qualitative profile of Raman spectra in different parts of the brain that are in agreement with the histopathology results (Figure 5) and indicate that MENP administration and use of the described magnetic delivery process are safe in animals. However, it should be noted that differences in the intensity of the Raman peaks' "quantitative information" is primarily because the MENPs are not uniformly distributed throughout the entire brain. We have previously demonstrated using TEM and inductively coupled plasma mass spectroscopy (ICPMS) the validation of efficient delivery of the MENPs using the magnetically guided CNS delivery approach in mice.[1] Replacement of the laborious and time-intensive *in situ* TEM, ICPMS, and histopathology techniques by Raman spectroscopy would allow timely investigation, for example, as an intraoperative surgery tool. This novel combination of modalities is our vision behind the integration of Raman and MRI analysis.

The generation of an aligned and focused magnetic field to deliver MENPs to a specific brain region or location to target specific localized brain lesions would be another significant advantage over the current neurotechnologies such as creating an opening in the BBB with focused ultrasound assistance and direct nanomedicine injection in the cerebral space. Such approaches seem less ideal for CNS disease treatment due to the invasiveness of the methods and possibility of creating neuroinflammatory agents, resulting in viral or dementia progression and motor coordination function.[34–37]

The Raman microscopic images (Figure 6e–g) and the spectroscopy (spectrum data not shown) of the peripheral organs provide the following important information: (a) magnetic delivery of the MENPs caused no physical damage to the cells and (b) MENPs are eventually cleared from the baboon via renal and hepatobiliary excretion in 30 days. Although magnetic hyperthermia has been widely studied and recognized by the National Cancer Institute for its clinical applications, the MENP technology is based on the "non-thermal" physical phenomenon of spintronics and magnetomechanics.[15] Intact morphology of the cells in the brain and the peripheral tissue indicated no cellular damage due to MENP presence along with an application of a high MRI magnetic field (Figure 6, in correlation and supported by histology analysis).

It should also be noted that traditional intravenous drug delivery technologies that rely on increased circulation time for nanomedicine follow two approaches: (a) coating of polymer around inorganic NCs to avoid opsonization, for example, dextran-coated magnetic

nanoparticles (MNPs),[38] and (b) time-consuming and potentially delayed targeted delivery. In the latter approach, the extended plasma half-life could be a constraint when delivering nanomedicine to the brain as prolonged circulation time increases the chances of premature drug release outside the targeted cerebral space. Our MENP-based drug delivery technology is an active delivery methodology wherein NF delivered to the brain within 3 h and, therefore, increased therapeutic significance.

Raman microscopy of the peripheral organs (Figure 6) indicated the presence of MENPs in several nonbrain regions, even after 30 days postinjection. The Raman morphology and correlation with the spectrum provide a possible understanding of the homeostatic conditions. Raman image analyses of the heart, lung, and spleen did not show any spectral signal related to the MENP presence (Figure 6e). We believe that the MENPs were cleared from the body through the renal excretory pathway (primary) and hepatic metabolic pathway (secondary), which is in agreement with the clearance properties seen with traditional magnetic nanoparticles such as iron oxide.[38–40] The clearance of MENPs through renal pathways involved the adrenal glands, uterus, bladder, and kidney (Figure 6f), and hepatic clearance involved the liver, stomach, and intestine (Figure 6g), signifying a possible clinical utility of MENPs. Although we are not certain about the exact route involved in MENP secretion, Raman studies suggested that MENP secretion may involve these nonurinary structures. Keeping this in view, various studies are in progress to confirm the exact route of MENP secretion from the baboon. Rapid renal clearance is the physiologically preferable pathway because it avoids involvement of cellular metabolism, which could otherwise lead to undesirable side effects. Like traditional MNP-based NFs, MENPs with a size <30 nm can be oxidized over time and begin to shrink into a smaller size ≤8 nm, which is the cutoff size for glomerulus filtration.[40] MENPs and other magnetic nanomedicine with sizes >30 nm and their opsonized aggregates are physiologically eliminated through the reticulo-endothelial system, primarily by the metabolic action of the liver's Kupffer cells and hepatocytes.[40] The metabolic byproduct of MENPs, iron, is likely to be either stored as body iron for use in physiological functions, such as heme content of hemoglobin, or eliminated through hepatobiliary excretion.[39] The results of Raman studies are in agreement with MRI imaging, and H&E staining outcomes strongly suggest that MENPs are a suitable NC for brain delivery (via MRI assistance) of NF developed for specific CNS diseases.

This brings the idea that the animal was not perfused at the sanctify time, and we are considering the possibility of MENP adherence to the walls.

VIEWPOINT

The primary aim of this study was to demonstrate the feasibility of a magnetically guided delivery of magneto-electric nanoparticles (MENPs) to the brain in a large animal model using MRI as a navigational tool. Being a pilot study and considering the study logistics, large animal availability, and coordinating a dedicated MRI, the present research is based on only one animal but the findings are of high significance as they could help in developing a human-compatible drug delivery module.

As a proof of the concept, the biodistribution of MENPs in the brain of the baboon was evaluated qualitatively. However, the quantitative estimation of the presence of MENPs in the brain of the baboon is lacking due to adopted scanning method limitations. However, this will be the main focus of future research which will be a time-intensive exercise. However, using this pilot study, we were successful in delivering MENPs to the brain of a nonhuman primate using MRI as a navigation tool to confirm delivery based on qualitative assessment. Besides qualitative confirmation of MENP delivery, the biosafety aspects of MENPs were also confirmed using histopathology, blood toxicity, and Raman spectroscopy. In the future, more studies will be planned to explore quantitative biodistribution of MENPs in the brain of nonhuman primates.

The findings of this research provide confidence to help scale-up this approach for targeted brain disease treatments. Aiming to make a human-compatible CNS disease therapy, the future focus of our work will be to develop a nanomedicine for eradication and management of neuroHIV in the setting of drug abuse using a monkey model.

CONCLUSIONS

Overall, the brain delivery method presented in this study is a human-compatible and noninvasive method to deliver nanoparticles across the BBB. The static magnetic field of the MRI successfully delivered MENPs to the brain of a Hamadryas baboon without adverse effects. The MENP presence in different regions of the brain was confirmed by MRI brain imaging. Analytical results of the brain, as well as peripheral tissue morphology and integration, along with blood profile toxicity, confirmed the safety of MENPs for future biomedical applications. Ferroelectric MENPs can be used for deep brain stimulation and on-demand release of specific drugs by applying external stimulation. This study can be a potential nanotherapeutic approach to targeting and treating many different CNS diseases that were previously considered difficult or impossible to manage and cure.

EXPERIMENTAL SECTION

Synthesis and Characterization of MENPs.

The MENPs utilized in this research were synthesized using a hydrothermal-assisted coprecipitation method as described in our previous report.[1,13,41] The synthesized nanoparticles were characterized using various analytical methods: for example, the crystalline nature of MENPs was evaluated using XRD study, the particle size was estimated using TEM imaging, and the biocompatibility of MENPs was assessed through examining cell viability of primary human astrocytes and SKNMC cells as a function of varying MENP concentrations using MTT assay.[1,41]

MRI-Responsive Characterization of MENPs.

To measure to relaxivities of MENPs as a function of concentration, a phantom study was performed. The known concentration of MENPs (10 to 500 μg) was suspended in agarose gel solution at 0.3% (50 mL) and heated at 40 °C in a beaker with stirring. Each composition of MENP/agarose gel was transferred in a plastic tube and allowed to cool at 4 °C for gel solidification.[42] The MENPs/agarose gel tubes were placed in the MRI (SIEMENS 3T)

machine for imaging. The T_2 and T_2* values were measured to establish a relation between varied magnitude as a function of different MENP concentration.

Optimization of Magnetic Exposure Time for Brain Delivery.

Based on the MTT assay, a dose of MENPs as 10 mg/mL was selected as a nontoxic and suitable concentration for injection in mice.[1] The MENPs were suspended in 100 μL of buffer and administrated intravenously to the mice while under general anesthesia. After MENP injection, each mouse was placed in a static magnetic field (0.8 T) for magnetically guided brain delivery.[1] The MENP-injected mice were harvested to perform *ex vivo* brain and liver MRI studies, using a 3.0 T Siemens TRIO TIM MRI (Siemens Medical Solutions USA, Malvern, PA) to evaluate the delivery and presence of MENPs as a function of time. For each time point studied, three mice were used for MENP injection and *ex vivo* MRI imaging. This study was performed to optimize the minimum period of time required to achieve maximum brain delivery efficacy. All of the experiments were carried out in accordance with relevant guidelines and regulations and approved by the Institutional Animal Care and Use Committee (IACUC) of Florida International University (FIU).

MRI-Assisted MENP Delivery to the Baboon Brain.

A female baboon was selected for this study. She was part of a different study prior to initiation but was clinically normal and healthy for this experiment. The animal was housed at the AAALAC-accredited animal care facility of University of Miami in accordance with the *Guide for the Care and Use of Laboratory Animals*.[43] The IACUC protocol for this study was approved by the University of Miami's Institutional Animal Care and Use Committee.

For the experiment, the baboon was anesthetized with ketamine hydrochloride (10 mg/kg intramuscularly) and maintained using isoflurane anesthesia. Two 18-gauge catheters were placed: one in each saphenous vein. One was placed for constant hydration maintenance and nanoparticle delivery, and one was kept for redundancy and emergency venous access if necessary. Once catheterized, the baboon was intubated with a 5.5 mm endotracheal tube and placed on isoflurane anesthesia with mechanical ventilation.

Once the baboon was under a stable anesthesia, a baseline MRI was performed using a 3.0 T Siemens TRIO TIM MRI (Siemens Medical Solutions USA, Malvern, PA). A 15 knee channel transmit/receive coil was used to image the brain for optimal signal-to-noise images. A 16-channel cardiac array surface coil was used to image the liver, spleen, and kidneys. The animal was monitored with a 3 T compatible wireless system from In-vivo Corporation (Gainesville, FL) using ECC, Pulse Ox, SPO2, and temperature monitors. A ventilator system Engler A.D.S. 1000 (Hialeah, FL) was used to keep the animals anesthetized during the imaging. Axial images of the brain and abdomen were obtained using a T_2* multiecho gradient recalled echo (GRE) sequence with TR = 210 ms, TE = 3, 6, 9, 12, 15, 18, and 21 ms, slice thickness = 4 mm with 0.4 mm gap, FOV = 200 × 150 mm, and in-plane matrix of 192 × 100. The pre- and post-injection scanning parameters utilized in this study were as follows: TR, 100; TE, 2.7–8.7; FA, 25; FOV, 120; Av, 4; Sl, 14; BW, 350; Res, 128 × 128; Voxel, 0.9 × 0.9 × 4. During the MRI measurements, appropriate body temperature was maintained via a Bair Hugger (3M, St. Paul, MN). Anesthesia was stable and maintained

throughout the entire procedure. After the MRI, the animal was removed from the MRI suite and maintained on isoflurane anesthesia. An amount of 22 mg of MENPs was dissolved in 100 mL of 0.9% normal saline and given IV over a period of 30 min via a peristaltic syringe pump at a controlled flow rate. The MENPs are visible in the solution, so occasional rocking of the fluid bag was utilized to ensure consistent delivery. Once the bag was empty, 20 mL of sterile 0.9% normal saline was placed into the bag and used to flush the IV line so that no nanoparticles remained within the administration system.

The animal was then placed back into the MRI and positioned with her head close to the magnet. Even when the MRI is not collecting images, the magnetic field is still present, and this was used to magnetically pull the nanoparticles across the BBB. The baboon remained in the MRI machine for 3 h to ensure the maximum amount of nanoparticles was transported across the BBB. After the 3 h of particle delivery, the MRI was used to take another image for the detection of the MENPs delivery and its distribution within the brain. After this second MRI, the baboon was recovered from anesthesia and taken back to its home cage and monitored. There were no clinical abnormalities (physical or neurobehavioral) seen during the entire treatment and recovery period. We have demonstrated MRI-assisted MENP delivery to the brain of the baboon twice, and the outcomes of MRI imaging are identical. Regular visual and behavioral exams were performed by the clinical veterinarian or by the research staff over the following 4 months, after the first injection.

For the second phase of experiments, the procedure was repeated exactly as described above. MRI imaging was utilized preinfusion, postinfusion, and then 7 days postinfusion, and then a terminal MRI was conducted immediately prior to euthanasia. Blood and urine were collected and submitted for routine analyses to the University of Miami's Comparative Pathology Laboratory pre- and postinfusion and then again on days 2, 7, 14, 21, and 30. During this time, the animal was checked daily by the clinical veterinarian or technicians for any evidence of clinical abnormalities, particularly neurobehavioral changes. No changes in the animal were observed, and the animal remained clinically normal throughout the entire study.

Blood Toxicity Analysis.

To evaluate the blood toxicity profile (in triplicate for each time point) of the MENP-injected baboon, a blood sample was collected after the injection at days 2, 7, 14, 21, and 30. All of the metabolic parameters studied were performed by the Department of Pathology at the University of Miami, Miami, USA. A preinjection blood sample was also collected and used as a control. The outcomes, in terms of varying enzyme levels, were analyzed with respect to the physiological range provided by the Department of Pathology.

Histopathology of the MENP-Injected Baboon.

On post-infusion day 30, the animal was euthanized with an intravenous overdose of pentobarbital sodium and phenytoin (Euthasol, Virbac AH, Inc., Ft. Worth, TX, USA) in accordance with AVMA guidelines.[44] Traditional necropsy organ tissue samples were collected for histopathology and included brain, liver, kidney, spleen, lung, heart, uterus, adrenal gland, bladder, stomach, and intestinal samples. The organs were cryopreserved

in 20% sucrose, embedded in Tissue Tek optimal cutting temperature compound (Sakura Finetek, Torrance, CA, USA), and used for histology and then imaged as described Rodriguez et al.[45] Briefly, tissue sections of 5–10 μm thickness were exposed to xylene and rehydrated with 95 and 70% ethanol, followed by staining with hematoxylin dye for 15 min and then eosin for 20 s. Tissues were then cleaned by xylene and mounted using mounting media for visualization. Images were acquired using a Zeiss (Germany) inverted fluorescence microscope with a 560 Axiovision camera using 40× objectives.[45] The histopathological evaluations were based on the guidelines of the *Society of Toxicologic Pathology*,[46] and the analysis of tissue morphology and toxicity was assessed by the Department of Pathology at the University of Miami, USA.

Raman Spectra and Image Acquisition from the Brain and Peripheral Organs.

Raman spectra and bright-field images were acquired using Raman spectro-microscopy from PerkinElmer, Raman station 400 F spectrometer integrated to Microscope 300. The images of the sample area were captured first, and then the spectra from that region were acquired. The Raman scanning mode was used to acquire at least five spectra per region using a 785 nm laser and 20× objective lens (backscattering) with spot size 100 μm, depth of field 250 μm, and laser power <100 mW at the sample with a 2 s laser exposure time. The spectra were processed using spectrum software to remove fluorescence and correct the baseline.

Supplementary Material

Refer to Web version on PubMed Central for supplementary material.

ACKNOWLEDGMENTS

The authors would like to acknowledge funding from NIH grants (R01DA042706, R01DA040537, R01DA037838, and R01DA034547). The authors also acknowledge the research facilities of the Institute of NeuroImmune Pharmacology (INIP) and Advanced Materials Engineering Research Institute (AMERI) of Florida International University. All the animal experiments were carried out in accordance with relevant guidelines and regulations and approved by IACUC of FIU and the University of Miami, respectively.

REFERENCES

(1). Kaushik A; Jayant RD; Nikkhah-Moshaie R; Bhardwaj V; Roy U; Huang Z; Ruiz A; Yndart A; Atluri V; El-Hage N; et al. Magnetically guided central nervous system delivery and toxicity evaluation of magneto-electric nanocarriers. Sci. Rep. 2016, 6, 25309. [PubMed: 27143580]

(2). Tomitaka A; Kaushik A; Kevadiya BD; Mukadam I; Gendelman HE; Khalili K; Liu G; Nair M.Surface-engineered multimodal magnetic nanoparticles to manage CNS diseases. Drug Discovery Today 2019, 24 (3), 873–882. [PubMed: 30660756]

(3). Kaushik A; Yndart A; Atluri V; Tiwari S; Tomitaka A; Gupta P; Jayant RD; Alvarez-Carbonell D; Khalili K; Nair M.Magnetically guided non-invasive CRISPR-Cas9/gRNA delivery across blood-brain barrier to eradicate latent HIV-1 infection. Sci. Rep. 2019, 9 (1), 3928. [PubMed: 30850620]

(4). Nair M; Jayant RD; Kaushik A; Sagar V.Getting into the brain: potential of nanotechnology in the management of Neuro-AIDS. Adv. Drug Delivery Rev. 2016, 103, 202–217.

(5). Vigo D; Thornicroft G; Atun R.Estimating the true global burden of mental illness. Lancet Psychiatry 2016, 3 (2), 171–178. [PubMed: 26851330]

(6). Kaushik A; Jayant RD; Bhardwaj V; Nair M.Personalized nanomedicine for CNS diseases. Drug Discovery Today 2018, 23 (5), 1007–1015. [PubMed: 29155026]

(7). Kaushik A; Jayant RD; Nair M.Nanomedicine for neuroHIV/AIDS management. Nanomedicine 2018, 13 (7), 669–673. [PubMed: 29485351]

(8). Jayant RD; Tiwari S; Atluri V; Kaushik A; Tomitaka A; Yndart A; Colon-Perez L; Febo M; Nair M.Multifunctional Nanotherapeutics for the Treatment of neuroAIDS in Drug Abusers. Sci. Rep. 2018, 8 (1), 12991. [PubMed: 30154522]

(9). Kaushik A; Jayant RD; Sagar V; Nair M.The potential of magneto-electric nanocarriers for drug delivery. Expert Opin. Drug Delivery 2014, 11 (10), 1635–1646.

(10). Wong HL; Wu XY; Bendayan R.Nanotechnological advances for the delivery of CNS therapeutics. Adv. Drug Delivery Rev. 2012, 64 (7), 686–700.

(11). Kaushik A; Jayant RD; Nair M.Advancements in nano-enabled therapeutics for neuroHIV management. Int. J. Nanomed. 2016, 11, 4317.

(12). Guduru R; Liang P; Runowicz C; Nair M; Atluri V; Khizroev S.Magneto-electric nanoparticles to enable field-controlled high-specificity drug delivery to eradicate ovarian cancer cells. Sci. Rep. 2013, 3, 2953. [PubMed: 24129652]

(13). Nair M; Guduru R; Liang P; Hong J; Sagar V; Khizroev S.Externally controlled on-demand release of anti-HIV drug using magneto-electric nanoparticles as carriers. Nat. Commun. 2013, 4, 1707. [PubMed: 23591874]

(14). Rodriguez M; Kaushik A; Lapierre J; Dever SM; El-Hage N; Nair M.Electro-Magnetic Nano-Particle Bound Beclin1 siRNA Crosses the Blood-Brain Barrier to Attenuate the Inflammatory Effects of HIV-1 Infection in Vitro. Journal of Neuroimmune Pharmacology 2017, 12 (1), 120–132. [PubMed: 27287620]

(15). Stimphil E; Nagesetti A; Guduru R; Stewart T; Rodzinski A; Liang P; Khizroev S.Physics considerations in targeted anticancer drug delivery by magnetoelectric nanoparticles. Appl. Phys. Rev. 2017, 4 (2), 021101.

(16). Nikkhah-Moshaie R; Kaushik A; Jayant RD; Bhardwaj V; Nair M.TEM Investigation of Nanocarriers Distribution in Mice Brain. Microsc. Microanal. 2016, 22 (S3), 1172–1173.

(17). Mathieu J; Beaudoin G; Martel S.Method of propulsion of a ferromagnetic core in the cardiovascular system through magnetic gradients generated by an MRI system. IEEE Trans. Biomed. Eng. 2006, 53 (2), 292–299. [PubMed: 16485758]

(18). Jermyn M; Mok K; Mercier J; Desroches J; Pichette J; Saint-Arnaud K; Bernstein L; Guiot M-C; Petrecca K; Leblond F.Intraoperative brain cancer detection with Raman spectroscopy in humans. Sci. Transl. Med. 2015, 7, No. 274.

(19). Kircher MF; De La Zerda A; Jokerst JV; Zavaleta CL; Kempen PJ; Mittra E; Pitter K; Huang R; Campos C; Habte F; et al. A brain tumor molecular imaging strategy using a new triple-modality MRI-photoacoustic-Raman nanoparticle. Nat. Med. 2012, 18 (5), 829–834. [PubMed: 22504484]

(20). Wu L-Q; Dickman JD Magnetoreception in an avian brain in part mediated by inner ear lagena. Curr. Biol. 2011, 21 (5), 418–423. [PubMed: 21353559]

(21). Ward BK; Tan GX; Roberts DC; Della Santina CC; Zee DS; Carey JP Strong static magnetic fields elicit swimming behaviors consistent with direct vestibular stimulation in adult zebrafish. PLoS One 2014, 9 (3), No. e92109. [PubMed: 24647586]

(22). Wu L-Q; Dickman JD Neural correlates of a magnetic sense. Science 2012, 336 (6084), 1054–1057. [PubMed: 22539554]

(23). Ward BK; Roberts DC; Della Santina CC; Carey JP; Zee DS Magnetic vestibular stimulation in subjects with unilateral labyrinthine disorders. Frontiers in neurology 2014, 5, 28. [PubMed: 24659983]

(24). Chakeres DW; de Vocht F.Static magnetic field effects on human subjects related to magnetic resonance imaging systems. Prog. Biophys. Mol. Biol. 2005, 87 (2), 255–265. [PubMed: 15556664]

(25). Nair AB; Jacob S.A simple practice guide for dose conversion between animals and human. Journal of basic and clinical pharmacy 2016, 7 (2), 27. [PubMed: 27057123]

(26). Sandino CM; Kellman P; Arai AE; Hansen MS; Xue H.Myocardial T2* mapping: influence of noise on accuracy and precision. Journal of Cardiovascular Magnetic Resonance 2015, 17 (1), 7. [PubMed: 25648167]

(27). Wood JC Magnetic resonance imaging measurement of iron overload. Curr. Opin. Hematol. 2007, 14 (3), 183. [PubMed: 17414205]

(28). Soenen SJ; Rivera-Gil P; Montenegro J-M; Parak WJ; De Smedt SC; Braeckmans K.Cellular toxicity of inorganic nanoparticles: common aspects and guidelines for improved nano-toxicity evaluation. Nano Today 2011, 6 (5), 446–465.

(29). Fadeel B; Garcia-Bennett AE Better safe than sorry: understanding the toxicological properties of inorganic nanoparticles manufactured for biomedical applications. Adv. Drug Delivery Rev. 2010, 62 (3), 362–374.

(30). Díaz B; Sańchez-Espinel C; Arruebo M; Faro J; de Miguel E; Magadań S; Yagüe C; Fernańdez-Pacheco R; Ibarra MR; Santamaría J.Assessing methods for blood cell cytotoxic responses to inorganic nanoparticles and nanoparticle aggregates. Small 2008, 4 (11), 2025–2034. [PubMed: 18855973]

(31). Bhardwaj V; Srinivasan S; McGoron AJ Efficient intracellular delivery and improved biocompatibility of colloidal silver nanoparticles towards intracellular SERS immuno-sensing. Analyst 2015, 140 (12), 3929–3934. [PubMed: 25939798]

(32). Scientific H.Raman Imaging of monkey brain tissue; HORIBA Jobin Yvon: France; 2014: pp 1–2.

(33). Tay L-L; Tremblay RG; Hulse J; Zurakowski B; Thompson M; Bani-Yaghoub M.Detection of acute brain injury by Raman spectral signature. Analyst 2011, 136 (8), 1620–1626. [PubMed: 21369597]

(34). Thomsen G; Alkaslasi M; Vit J; Lawless G; Godoy M; Gowing G; Shelest O; Svendsen C.Systemic injection of AAV9-GDNF provides modest functional improvements in the SOD1G93A ALS rat but has adverse side effects. Gene Ther. 2017, 24 (4), 245. [PubMed: 28276446]

(35). Golebiowski D; van der Bom IM; Kwon C-S; Miller AD; Petrosky K; Bradbury AM; Maitland S; Kühn AL; Bishop N; Curran E; et al. Direct Intracranial Injection of AAVrh8 Encoding Monkey β-N-Acetylhexosaminidase Causes Neurotoxicity in the Primate Brain. Hum. Gene Ther. 2017, 28 (6), 510–522. [PubMed: 28132521]

(36). Wang S; Karakatsani ME; Fung C; Sun T; Acosta C; Konofagou E.Direct brain infusion can be enhanced with focused ultrasound and microbubbles. J. Cereb. Blood Flow Metab. 2017, 37, 706. [PubMed: 26969468]

(37). Gill SS; Patel NK; Hotton GR; O'Sullivan K; McCarter R; Bunnage M; Brooks DJ; Svendsen CN; Heywood P.Direct brain infusion of glial cell line-derived neurotrophic factor in Parkinson disease. Nat. Med. 2003, 9 (5), 589–595. [PubMed: 12669033]

(38). Bourrinet P; Bengele HH; Bonnemain B; Dencausse A; Idee J-M; Jacobs PM; Lewis JM Preclinical safety and pharmacokinetic profile of ferumoxtran-10, an ultrasmall superparamagnetic iron oxide magnetic resonance contrast agent. Invest. Radiol. 2006, 41 (3), 313–324. [PubMed: 16481915]

(39). Jain TK; Reddy MK; Morales MA; Leslie-Pelecky DL; Labhasetwar V.Biodistribution, clearance, and biocompatibility of iron oxide magnetic nanoparticles in rats. Mol. Pharmaceutics 2008, 5 (2), 316–327.

(40). Longmire M; Choyke PL; Kobayashi H.Clearance properties of nano-sized particles and molecules as imaging agents: considerations and caveats. Nanomedicine 2008, 3, 703–717. [PubMed: 18817471]

(41). Kaushik A; Nikkhah-Moshaie R; Sinha R; Bhardwaj V; Atluri V; Jayant RD; Yndart A; Kateb B; Pala N; Nair M.Investigation of ac-magnetic field stimulated nanoelectroporation of magneto-electric nano-drug-carrier inside CNS cells. Sci. Rep. 2017, 7, 45663. [PubMed: 28374799]

(42). Billotey C; Wilhelm C; Devaud M; Bacri J; Bittoun J; Gazeau F.Cell internalization of anionic maghemite nanoparticles: quantitative effect on magnetic resonance imaging. Magn. Reson. Med. 2003, 49 (4), 646–654. [PubMed: 12652535]

(43). Council NR Guide for the care and use of laboratory animals; National Academies Press: 2010.

(44). Leary S; Underwood W; Anthony R; Cartner S; Corey D; Grandin T; Greenacre CB; Gwaltney-Bran S; McCrackin MA; Meyer R.AVMA guidelines for the euthanasia of animals; American Veterinary Medical Association: Schaumburg, IL, 2013.

(45). Rodriguez M; Lapierre J; Ojha CR; Kaushik A; Batrakova E; Kashanchi F; Dever SM; Nair M; El-Hage N.Intranasal drug delivery of small interfering RNA targeting Beclin1 encapsulated with polyethylenimine (PEI) in mouse brain to achieve HIV attenuation. Sci. Rep. 2018, 8, 4778. [PubMed: 29540788]

(46). Crissman JW; Goodman DG; Hildebrandt PK; Maronpot RR; Prater DA; Riley JH; Seaman WJ; Thake DC Best practices guideline: toxicologic histopathology. Toxicol. Pathol. 2004, 32 (1), 126–131. [PubMed: 14713558]

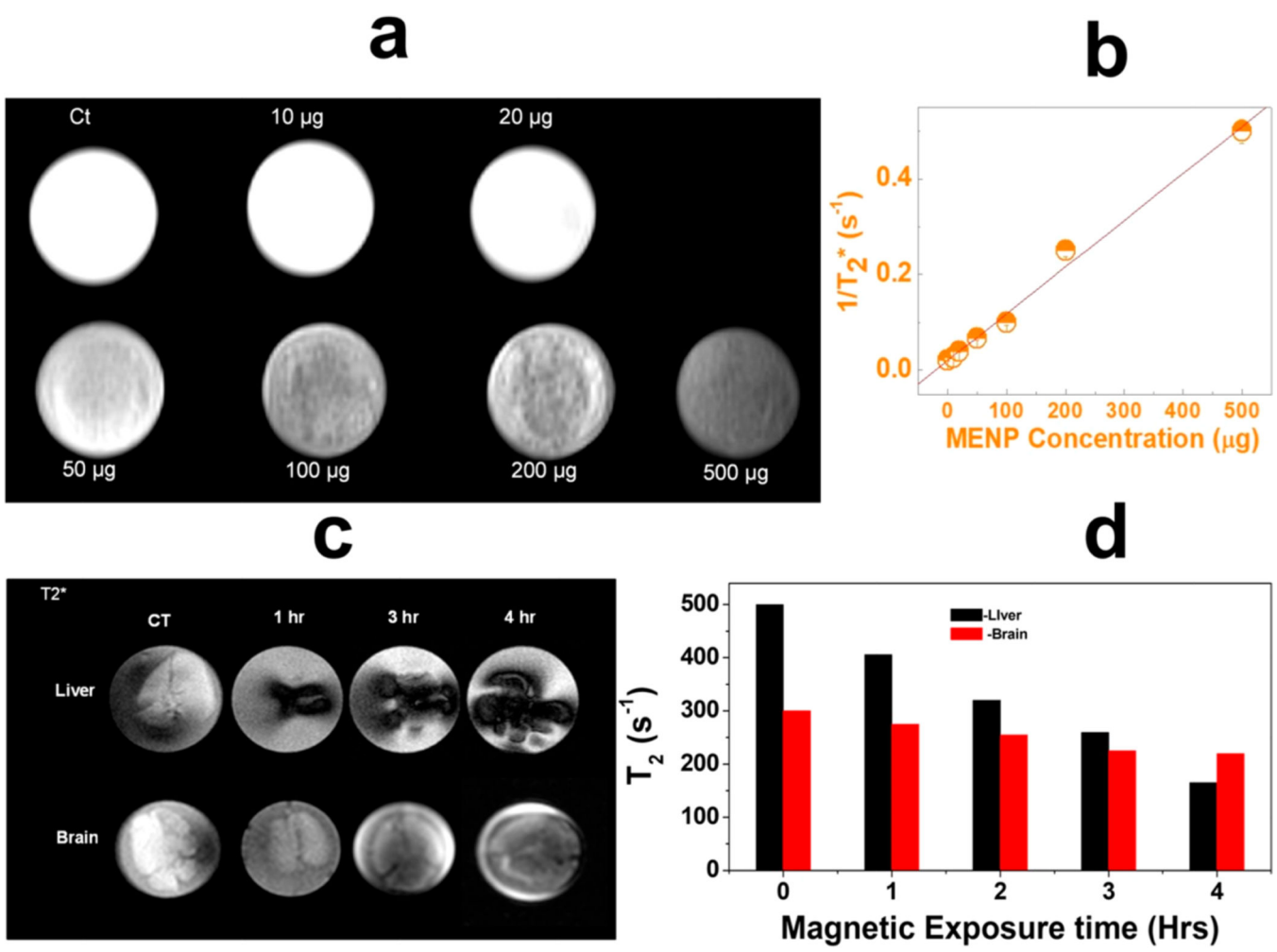

Figure 1.

MRI-responsive study of MENPs and magnetically guided brain delivery in the brain of mice. (a) *In vitro* MRI phantom study as a function of varied MENP concentration (10–500 mg) and a relation between contrast variation in terms of T_2 value as a function of MENP dose. (b) *Ex vivo* brain and liver MRI imaging of magnetically guided brain delivery of MENPs (10 mg/kg injected through intravenous administration) to the brain and liver of mice (c) and (d) relationship between tissue T_2 value variation and as a function of static magnetic exposure time.

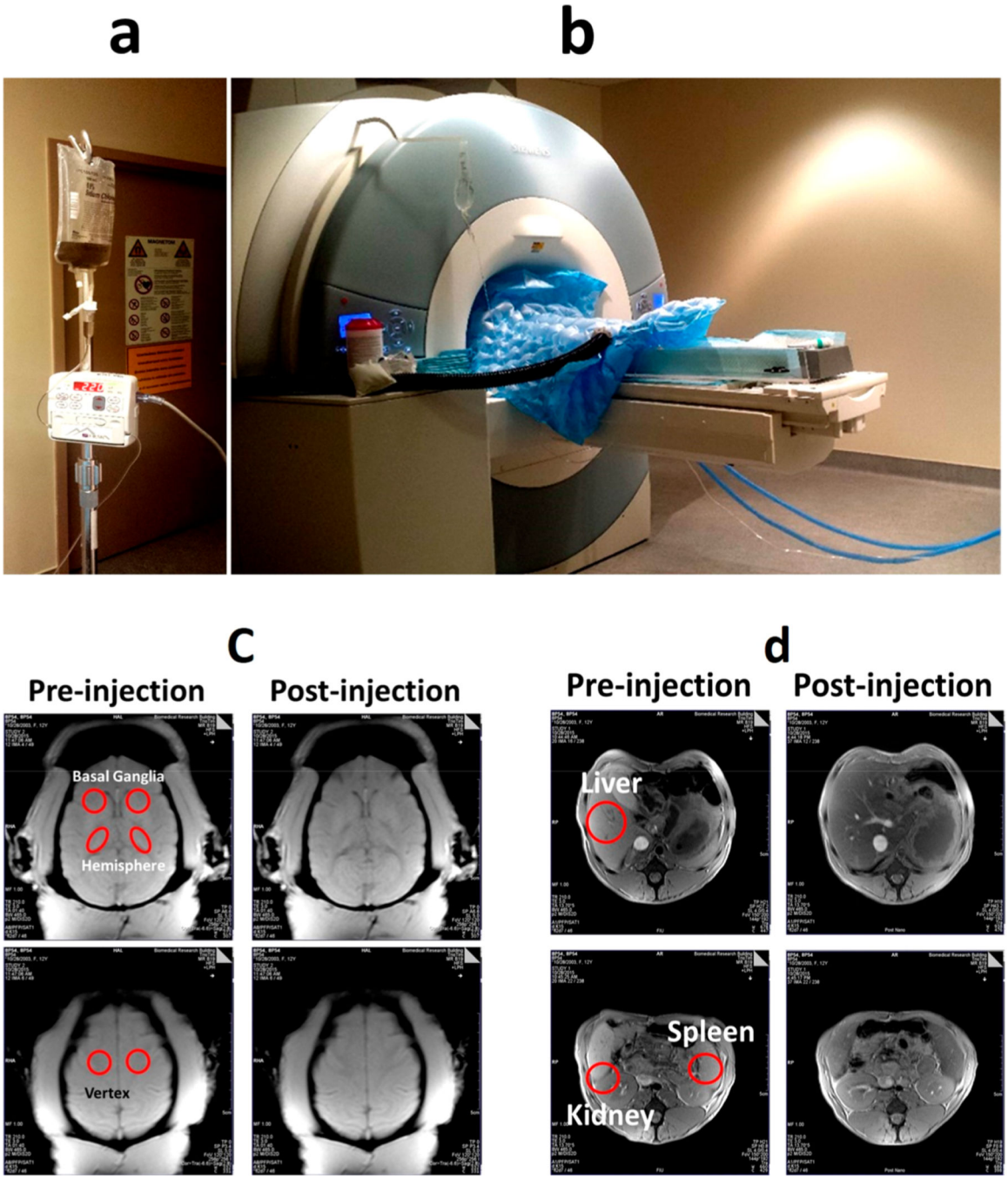

Figure 2.

MRI-assisted magnetically guided brain delivery of MENPs in the baboon. (a) Illustration of MENPs, suspended in 100 mL of PBS, administration in the baboon through a microfluidic pump, (b) magnetically guided brain delivery on MENPs to the brain of a female adult baboon using an MRI instrument as a navigation tool, (c) gray-scale MRI image of the basal ganglia, hemisphere, and vertex at pre/post MENP injection in the baboon, and (d) gray-scale MRI image of the liver, kidney, and spleen at pre/post MENP injection in the

baboon. These regions of interest do not show a significant difference in T_2 value and thus raise the demand of image processing to confirm the presence of MENPs in the brain.

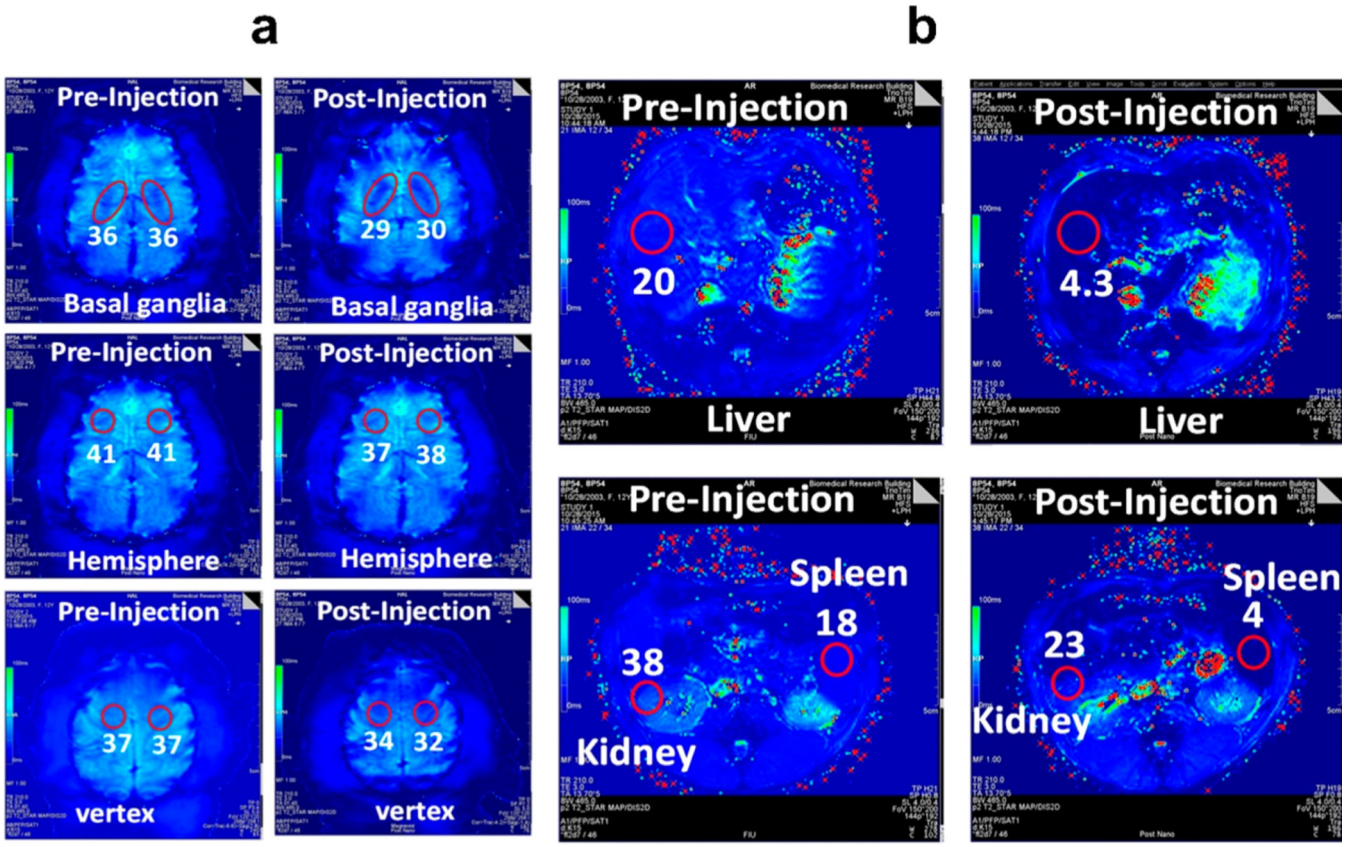

Figure 3.

Representation of T_2 value as a function of magnetic exposure time. In the brain, the T_2 value saturated after 3 h of exposure confirmed this as optimized magnetic exposure to achieve maximum brain delivery. (a) MRI-assisted brain delivery MENPs intravenously administrated in the baboon. MRI brain imaging of the MENP-injected baboon showed a significant reduction in T_2* value at the basal ganglia, hemisphere, and vertex and confirmed MRI-assisted brain delivery. (b) A significant reduction in T_2* value was also observed in the liver, kidney, and spleen.

a

Parameters	Physiological Range	Pre-injection	Post-injection				
			Day 2	Day 7	Day 14	Day 21	Day 30
Liver Function toxicity profile							
WBC	5.2 to 10.3 x 10^3/μL	8.0	6.9	8.2	11.5	5.2	8.3
RBC	5.2 to 6.0 x 10^6/μL	5.5	5.32	5.27	5.32	5.44	5.21
Hemoglobin	11.5 to 12.7 g/dL	11.4	11.20	10.9	11.5	11.5	10.8
Hematocrit	35 to 39 %	37	38	37	37	37	36
MCV	65-70 fL	67	71	70	70	67	69
MCH	21 to 23 pg	21	21	21	22	21	21
MCHC	31 to 35 %	31	30	29	31	31	30
Segmented Neutrophils	30 to 57 %	76	68	62	74	67	73
Band Neutrophils	0 to 2 %	0	0	0	0	0	0
Lymphocytes	36 to 64 %	19	29	30	16	23	25
Monocytes	0 to 3 %	2	3	2	2	2	2
Eosiniohils	0 to 6 %	3	0	6	8	8	0
Basophils	0 to 1 %	0	0	0	0	0	0
NRBC		0	0	0	0	0	0
RBC Morphology	Normal						
Platelet Morphology	Normal						
WBC morphology	Normal						

b

Parameters	Physiological Range	Pre-injection	Post-injection				
			Day 2	Day 7	Day 14	Day 21	Day 30
Renal Function toxicity profile							
Hemolysis Index	0	0					
Lipemia Index	0	0					
Glucose	47 to 65 mg/dL	75	89	71	76	73	63
BUN	15 to 21 mg/dL	18	13	15	15	11	29
CREA	0.5 to 0.9 mg/dL	0.7	0.7	0.5	0.6	0.8	0.7
BUN/CREA Ratio	23 to 30	22.5	18.6	30.0	25.0	13.8	41.4
Sodium	142 to 150 mmol/L	143	139	143	139	146	147
Potassium	3.3 to 3.8 mmol/L	4.0	4.1	3.6	4.2	4.4	4.2
Chloride	106 to 115 mmol/L	100	99	106	103	107	101
CO_2		28 mmol/L	30	30	24	28	29
Amylase		213 U/L	214	213	255	150	237
Calcium	8.5 to 9.3 mg/dL	9.1	9.6	8.8	9.1	9.9	10.5
Phosphorus	6.0 to 8.5 mg/dL	4.4	2.4	3	3.6	5.1	1.5
Cholesterol	114 to 151 mg/dL	99	88	98	89	135	88
Total Protein	6.8 to 7.5 g/dL	6.1	6.0	5.8	5.7	6.9	6.7
Albumin	4.0 to 4.4 g/dL	3.2	3.0	2.8	2.7	3.5	3.5
A/G Ratio	1.1 to 1.6	1.10	1.0	0.993	0.9	1.03	1.09
AST	19 to 48 U/L	43	28	44	30	24	30
ALT	27 to 55 U/L	51	62	60	44	51	53
Alkaline Phosphatase	89 to 470 U/L	180	199	175	197	223	191
Total Bilirubin	0.1 to 0.5 mg/dL	< 0.1	< 0.1	0.1	< 0.1	0.2	0.1

Figure 4.

Blood toxicity profile of the MENP-injected the baboon. Various important parameters of the liver (a) and renal (b) function toxicity profile were studied as a function of time after the MENP injection in the baboon. All the parameters were observed in the physiological range and suggested nontoxicity and biocompatibility of MENPs.

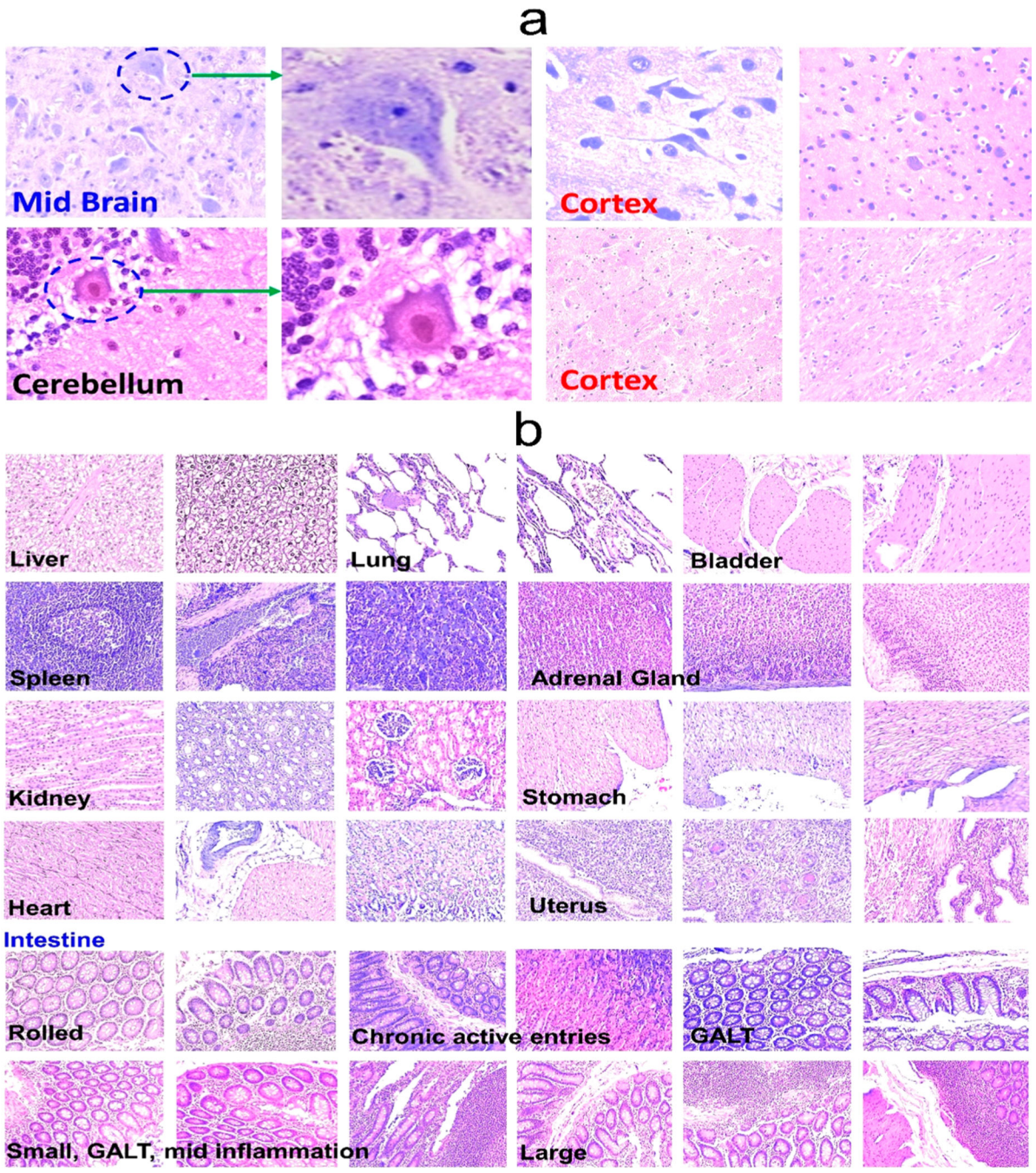

Figure 5.

Morphological assessment of MENP-injected baboon organs using hematoxylin eosin staining. (a) Representative images of different regions of the brain, including the midbrain, cerebellum, and frontal cortex at 20 X magnification. (b) Representation of H&E stained images of various peripheral organs including the liver, lung, bladder, spleen, adrenal gland, kidney, stomach, heart, uterus, and intestine.

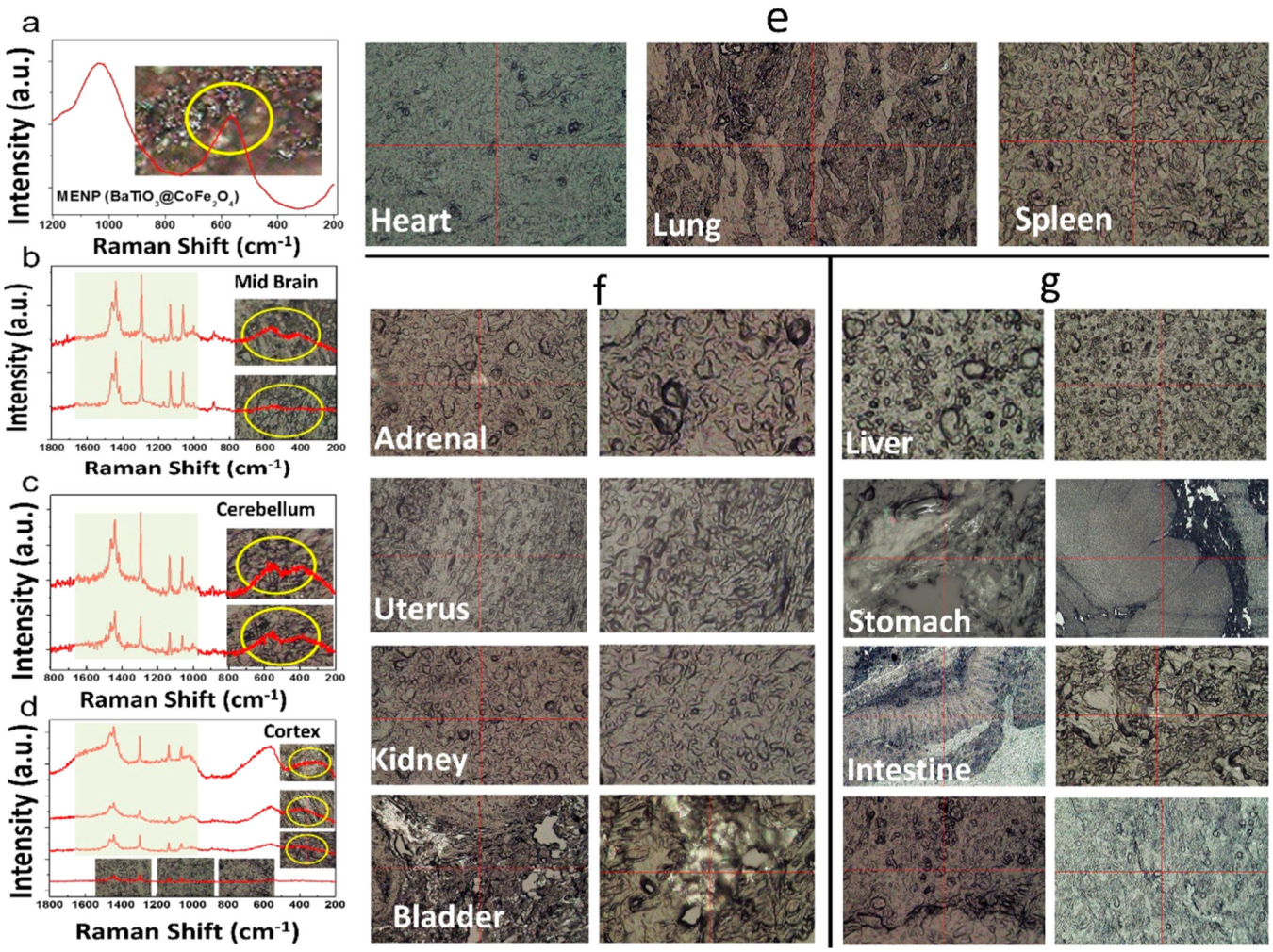

Figure 6.

Evaluation of integration of MENP-injected baboon tissues using Raman spectroscopy and microscopy. In the case of the brain, the fixed brain regions were analyzed using Raman microscopy for the visual inspection followed by Raman spectroscopy experiments at various locations to evaluate the effect of MENPs. Rama spectroscopy and microscopy of (a) MENPs, (b) midbrain, (c) cerebellum, and (d) cortex. Raman microscopy was utilized to explore the visual inspection of the (e) heart, lung, and spleen; (f) adrenal, uterus, kidney, and bladder; and g) liver, stomach, and intestine.